

Supplementary Material: Effect of Polymer Structure and Chemistry on Viscosity Index, Thickening Efficiency, and Traction Coefficient of Lubricants

Pawan Panwar ¹, Emily Schweissinger ², Stefan Maier ², Stefan Hilf ², Sofia Sirak ², and Ashlie Martini ^{1,*}

¹ Department of Mechanical Engineering, University of California Merced, 5200 N. Lake Road, Merced, CA 95343, USA

² Evonik Operations GmbH, Kirschenallee, 64293 Darmstadt, Germany

* Correspondence: amartini@ucmerced.edu

Section S1. Instruments

A Cannon StressTech HR Oscillatory Rheometer was used to measure dynamic viscosity at low shear rates, a generic viscometer was used to measure the kinematic viscosity, and a PCS Mini-Traction Machine was used to measure traction coefficients. Schematics of these devices are shown in Figure S1.

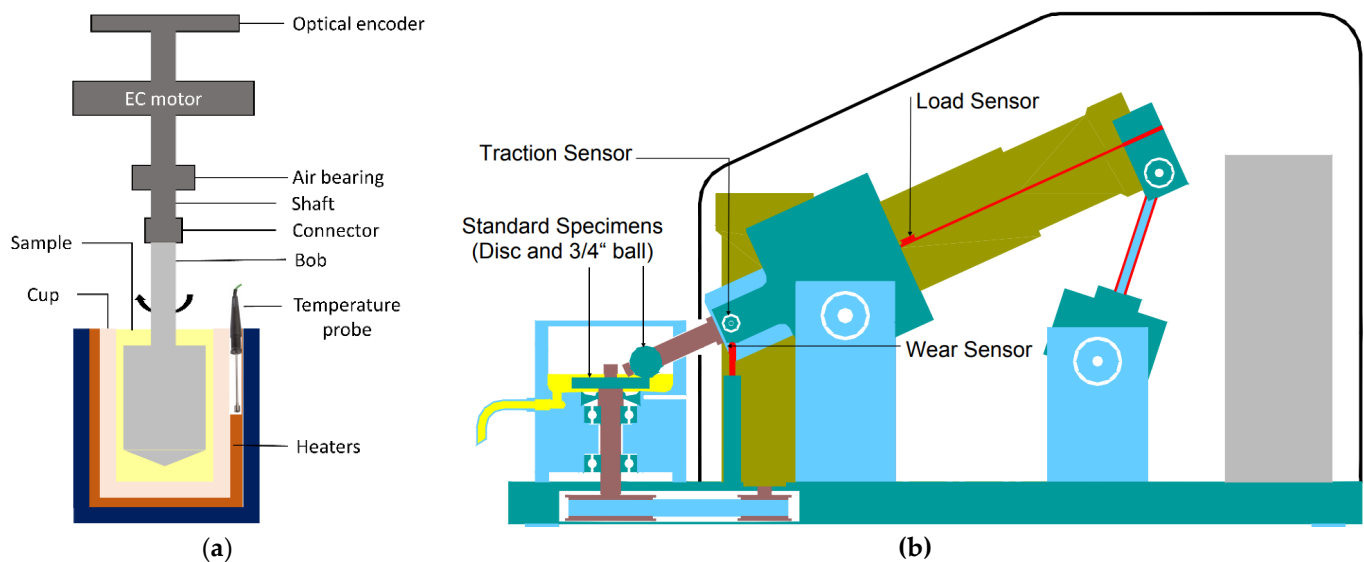


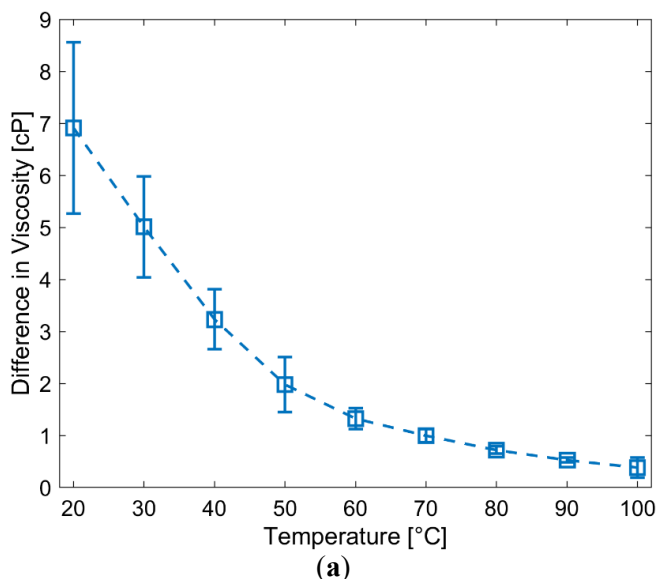
Figure S1. Schematics of (a) Cannon StressTech HR Oscillatory Rheometer and (b) PCS Mini-Traction Machine [1] used for measuring dynamic viscosity and traction coefficient, respectively.

Section S2. Experimental and Simulation Data

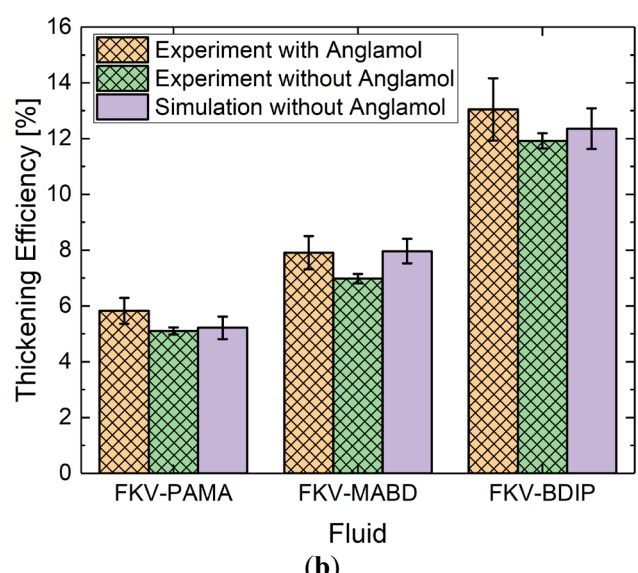
Listed in Table S1 are the experimental and simulated kinematic viscosity of all fluid with error at 40 and 100 °C. The asterisk indicates the kinematic viscosity measured for the fluids with additive package. The viscosity data listed in Table S1 and shown in Figure S2(a) show that the fluids formulated with 6.5 wt.% of Anglamol 99 additive package had higher viscosity than the fluids formulated without the additive package.

Table S1. Experimental and simulated viscosity of base oil and test fluids. The asterisk indicates the kinematic viscosity measured for the fluids with 6.5 wt.% of Anglamol 99 additive package.

Temperature [°C]	Fluid	Polymer, C [wt.%]	Viscosity [cSt]		
			Experiment*	Experiment	Simulation
40	Base Oil (PAO3cSt)	0.0	-	11.50 ± 0.31	11.74 ± 1.18
	FKV-PAO	15.7	34.08	-	34.31 ± 4.30
	FKV-PIB	14.6	35.60	-	33.25 ± 4.20
	FKV-BDIP	9.8	33.23 ± 0.39	30.81	28.64 ± 4.54
	FKV-PAMA	20.8	31.83 ± 0.33	28.69	27.61 ± 5.21
	FKV-MABD	15.8	32.78 ± 0.41	29.51	33.30 ± 4.81
100	Base Oil (PAO3cSt)	0.0	-	3.09 ± 0.18	3.14 ± 0.27
	FKV-PAO*	15.7	7.01	-	7.05 ± 0.80
	FKV-PIB	14.6	7.03	-	6.89 ± 0.53
	FKV-BDIP	9.8	7.06 ± 0.32	6.72	6.85 ± 0.62
	FKV-PAMA	20.8	6.86 ± 0.29	6.39	6.44 ± 0.77
	FKV-MABD	15.8	6.98 ± 0.28	6.52	7.00 ± 0.59



(a)



(b)

Figure S2. (a) Average increase in viscosity of the fluids when the fluids are formulated with 6.5 wt.% of Anglamol 99 additive package compared to the fluids formulated without the additive package. (b) Thickening efficiency calculated from experimentally measured viscosity of the fluids formulated with and without 6.5 wt.% of Anglamol additives package at 100°C, and from the simulation calculated viscosity of the fluids formulated without 6.5 wt.% of Anglamol additives package at 100°C.

This comparison in Figure S2(b) shows a consistent trend in thickening efficiency of fluids formulated with and without 6.5 wt.% of Anglamol additives package.

Listed in Table S2 are the experimental and simulated traction coefficients of all fluid at 40 °C and MTM test conditions. The asterisk indicates the traction coefficient measured for the fluids with additive package. The traction coefficient data listed in Table S2 shows that the fluids formulated with 6.5 wt.% of Anglamol 99 additive package had higher traction coefficient than the fluids formulated without the additive package.

Table S2. Experimental and simulated traction coefficient of test fluids. The asterisk indicates the traction coefficient measured for the fluids with 6.5 wt.% of Anglamol 99 additive package.

Fluid	Polymer, C [wt.%]	Traction Coefficient [-]		
		Experiment*	Experiment	Simulation
FKV-PAO	15.7	0.04550	-	0.05068
FKV-PIB	14.6	0.05900	-	0.06583
FKV-BDIP	9.8	0.04650	0.04460	0.05672
FKV-PAMA	20.8	0.04850	0.04720	0.06434
FKV-MABD	15.8	0.04780	0.04630	0.05796

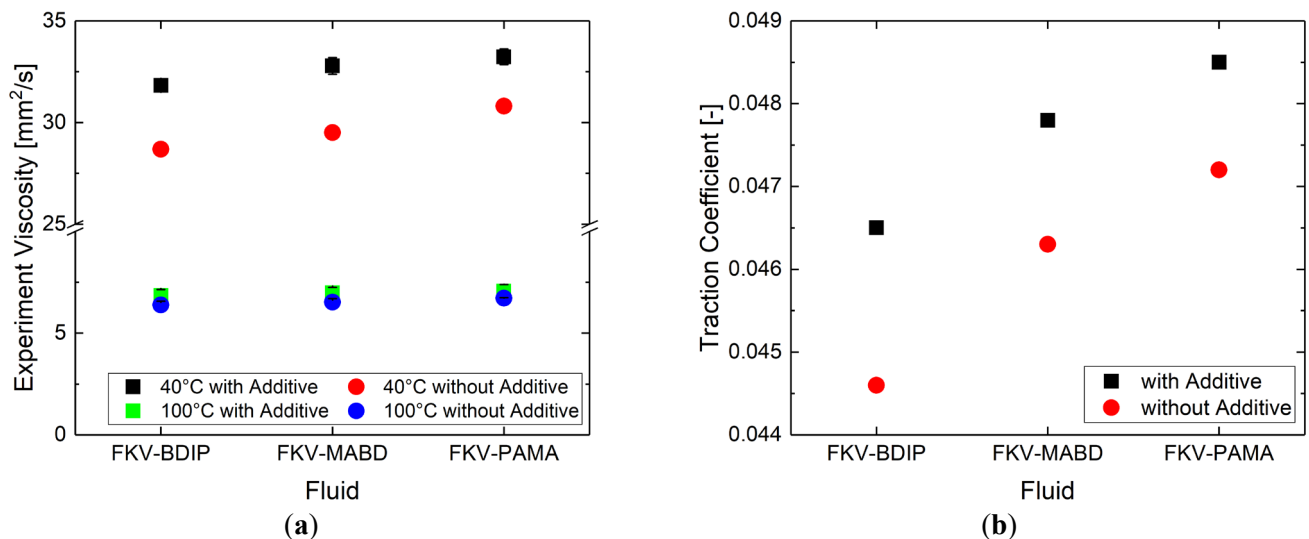


Figure S3. (a) Experimentally measured kinematic viscosity of the fluids formulated with and without 6.5 wt.% of Anglamol additives package at 40 and 100°C. (b) Experimentally measured traction coefficient of the fluids formulated with and without 6.5 wt.% of Anglamol additives package at 40°C.

This comparison in Figure S3 shows a consistent trend in viscosity and traction coefficient of fluids formulated with and without 6.5 wt.% of Anglamol additives package.

Section S3. Base Oil Formulation

Since the composition of group III 3 cSt base oil was unknown, an alternative 3 cSt base oil was formulated by blending 25 wt.% of 2 cSt PAO with 75 wt.% of 4 cSt PAO for the simulation. Previous gas chromatography-mass spectroscopy measurements reported that PAO2 consisted of nearly 100% 1-decene dimer C₂₀H₄₂ and PAO4 consisted of equal parts 1-decene trimer C₃₀H₆₂ and tetramer C₄₀H₈₂ [2]. Viscosity of the blended samples was measured at low shear rate of 50 1/s (that is, in Newtonian regime) at 40 and 100 °C using a Cannon StressTech HR Oscillatory Rheometer. The average and standard deviation are determined from 3 runs each of 2 blended samples of base oil. The properties of this 3 cSt PAO base oil are listed in Table 3. It must be noted here that all the fluids were simulated by blending polymers with this synthetic 3 cSt PAO base oil, however, physically blended fluids with polymers used group III 3 cSt base oil. The group III and group IV (i.e., PAO based base oils) have viscosity index (VI) as high as 120 and 140, respectively. This difference in the VI might have some impact on the viscosity index of the samples.

Table S3. Properties of 3 cSt PAO base oil blend.

Temperature [°C]	Avg. Viscosity [cP]	Std. Deviation [cP]	Density [g/cc]	Avg. Viscosity [cSt]
40	9.153	0.225	0.796	11.499
100	2.324	0.168	0.753	3.086

Table S4. Calculation of ratio of base oil molecules in the proposed 3 cSt PAO base oil.

25wt% PAO2 + 75wt% PAO4					
Molecule	PAO2		PAO4		Sum
	Dimer	Trimer	Tetramer		
Molar mass of each molecule, M_{oi} [g/mol]	282.5475	422.8133	563.0791	1268.4399	
Weight fraction of each molecule, w_i	0.2500	0.3750	0.3750	1.0000	
Mole of each molecule in 100 g, $n_i = w_i/M_{oi} \times 100$	0.0885	0.0887	0.0666	0.2438	
Total number of moles, $\sum n_i$	0.2438			0.2438	
Mole fraction of each molecule, $x_i = n_i/\sum n_i$	0.3630	0.3638	0.2732	1.0000	
Number of each molecule if total number of molecules in the simulation box is $N_T = 11$, $N_i = N_T \times x_i$	3.9926	4.0022	3.0052	11.0000	

Section S4. Simulation Plan

For all simulations, we tried to have around or more than 12000 UA in the simulation box of approximate dimension of $300.0\text{\AA} \times 30.0\text{\AA} \times 30.0\text{\AA}$. These criteria and desired formulation listed in Table S5 which decided how many polymers we should have in the simulation box for each fluid. As it can be seen from the dimension of simulation box, orthogonal simulation boxes were considered since these models were also sheared in the traction coefficients simulation.

Table S5. Simulation plan of each test fluids.

Fluid ID	Desired Formulation	Number of Molecules
FKV-PAO	<ul style="list-style-type: none"> • 15.7 wt.% PAO Polymer • 84.3 wt.% 3 cSt Base oil 	<ul style="list-style-type: none"> • 5 PAO polymer → 15.7 wt.% • 120 Dimers → 21.1 wt.% • 120 Trimers → 31.6 wt.% • 90 Tetramers → 31.6 wt.% • Box size = $296.4\text{\AA} \times 30.0\text{\AA} \times 30.0\text{\AA}$
FKV-PIB	<ul style="list-style-type: none"> • 14.6 wt.% PIB Polymer • 85.4 wt.% 3 cSt Base oil 	<ul style="list-style-type: none"> • 11 PIB polymer → 14.6 wt.% • 122 Dimers → 21.2 wt.% • 122 Trimers → 32.1 wt.% • 91 Tetramers → 32.1 wt.% • Box size = $252.9\text{\AA} \times 30.0\text{\AA} \times 30.0\text{\AA}$
FKV-BDIP	<ul style="list-style-type: none"> • 9.8 wt.% BDIP Polymer • 90.2 wt.% 3 cSt Base oil 	<ul style="list-style-type: none"> • 1 BDIP polymer → 9.8 wt.% • 132 Dimers → 22.6 wt.% • 132 Trimers → 33.8 wt.% • 100 Tetramers → 33.8 wt.% • Box size = $306.5\text{\AA} \times 30.0\text{\AA} \times 30.0\text{\AA}$
FKV-PAMA	<ul style="list-style-type: none"> • 20.8 wt.% PAMA Polymer • 79.2 wt.% 3 cSt Base oil 	<ul style="list-style-type: none"> • 1 PAMA polymer → 20.8 wt.% • 110 Dimers → 19.8 wt.% • 110 Trimers → 29.7 wt.% • 83 Tetramers → 29.7 wt.% • Box size = $289.5\text{\AA} \times 30.0\text{\AA} \times 30.0\text{\AA}$
FKV-MABD	<ul style="list-style-type: none"> • 15.8 wt.% MABD Polymer • 84.2 wt.% 3 cSt Base oil 	<ul style="list-style-type: none"> • 2 MABD polymer → 15.8 wt.% • 105 Dimers → 21.0 wt.% • 106 Trimers → 31.6 wt.% • 79 Tetramers → 31.6 wt.% • Box size = $260.5\text{\AA} \times 30.0\text{\AA} \times 30.0\text{\AA}$

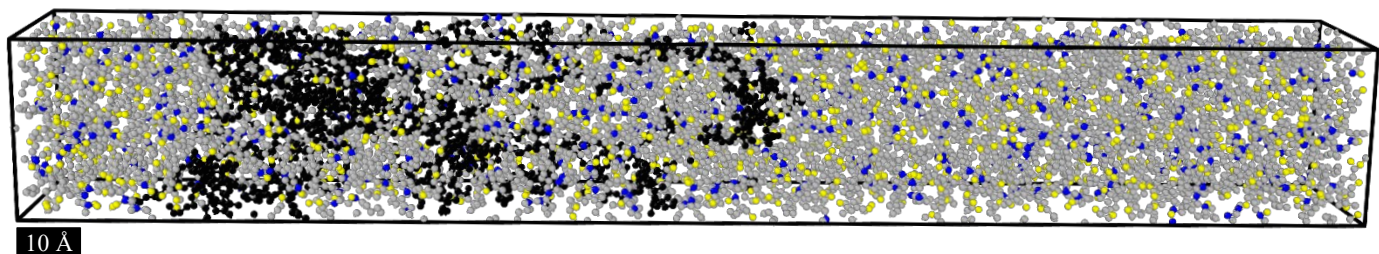


Figure S4. Simulation box representing FKV-MABD fluid. The cluster of black atoms represents MABD polymers and cluster of yellow, grey, and blue colors atoms represent base oil molecules (dimer, trimer, and tetramer of 1-decene). The longest side of box was considered x -direction in which shear was applied.

65
66
67
68
69

70

71
72
73
74
75
76

Section S5. Forcefield Parameters [3–12]

The TraPPE-UA forcefield was used to describe the chemistry of molecules. In the TraPPE-UA force field, the non-bonded interactions \mathbf{U}_{NB} between atoms which are separated by more than three bonds or belongs to different molecules are described by combination of pairwise-additive Lennard-Jones 12-6 potentials and electrostatic interactions by the Ewald summation, 1-2 bonded interactions \mathbf{U}_{bond} are considered to have fixed bond lengths, 1-3 bonded or bond angles interactions \mathbf{U}_{bend} are governed by harmonic potential, and the motion of the dihedral angle or 1-4 bonded interactions $\mathbf{U}_{torsion}$ is governed by Fourier potential. The original TraPPE uses fixed bond lengths, but to model fully flexible bonds, a harmonic potential was implemented by taking the corresponding force constants [10,13]. This fully flexible model can be described by Equation S1.

$$\mathbf{U}_{total} = \mathbf{U}_{bond}(\mathbf{r}) + \mathbf{U}_{bend}(\theta) + \mathbf{U}_{torsion}(\phi) + \mathbf{U}_{NB}(r_{ij}) \quad (S1)$$

$$\mathbf{U}_{bond}(\mathbf{r}) = \frac{k_r}{2} (\mathbf{r} - \mathbf{r}_0)^2 \quad (S2)$$

$$\mathbf{U}_{bend}(\theta) = \frac{k_\theta}{2} (\theta - \theta_0)^2 \quad (S3)$$

$$\mathbf{U}_{torsion}(\phi) = C_0 + C_1[1 + \cos(\phi)] + C_2[1 - \cos(2\phi)] + C_3[1 + \cos(3\phi)] + C_4[1 - \cos(4\phi)] \quad (S4)$$

$$U_{NB}(r_{ij}) = 4\epsilon_{ij} \left[\left(\frac{\sigma_{ij}}{r_{ij}} \right)^{12} - \left(\frac{\sigma_{ij}}{r_{ij}} \right)^6 \right] + \frac{q_i q_j}{4\pi\epsilon_0 r_{ij}} \quad (S5)$$

$$\sigma_{ij} = \frac{1}{2}(\sigma_{ii} + \sigma_{jj}) \quad \text{and} \quad \epsilon_{ij} = (\epsilon_{ii}\epsilon_{jj})^{1/2} \quad (S6)$$

Here, \mathbf{U}_{total} is the total interaction potential, \mathbf{U}_{bond} , \mathbf{U}_{bend} , $\mathbf{U}_{torsion}$, respectively are the potential of 1-2, 1-3, and 1-4 bonded interaction, and \mathbf{U}_{NB} is the total potential of nonbonded interactions due to both the pairwise and electrostatic interactions. \mathbf{r} is the distance between two bonded atoms, θ is the angle between three consecutively bonded atoms, ϕ is the torsional angle between four consecutively bonded atoms. Here, r_{ij} , ϵ_{ij} , and σ_{ij} are the separation, LJ well depth, and LJ size, respectively, for the pair of atoms i and j . For Lennard-Jones interactions between two different atom types, the standard Lorentz-Bethelot empirical combining rules were used to compute parameters using Equation S6.

It must be mentioned that TraPPE torsion potential parameters in some literatures were provided for either of the torsion potential of forms expressed by Equations S7 and S8.

$$\mathbf{U}_{torsion}(\phi) = \sum_{n=0,4} A_n \cos^n(\phi) = A_0 + A_1 \cos(\phi) + A_2 \cos^2(\phi) + A_3 \cos^3(\phi) + A_4 \cos^4(\phi) \quad (S7)$$

$$\mathbf{U}_{torsion}(\phi) = B_0 + B_1 \cos(\phi) + B_2 \cos(2\phi) + B_3 \cos(3\phi) + B_4 \cos(4\phi) \quad (S8)$$

These torsional potential parameters or coefficients were then converted using the following rigorous equivalences that were obtained by trigonometric transformations:

$$C_0 = A_0 - A_1 + A_2 - A_3 + A_4, \quad C_1 = A_1 + 3A_3/4, \quad C_2 = -(A_2 + A_4)/2, \quad C_3 = A_3/4, \quad \text{and} \quad C_4 = -A_4/8, \quad \text{or} \quad C_0 = B_0 - B_1 + B_2 - B_3 + B_4, \quad C_1 = B_1, \quad C_2 = -B_2, \quad C_3 = B_3, \quad \text{and} \quad C_4 = -B_4. \quad (S9)$$

The potential parameters that are used to fully describe these molecules by Equation S11 are given in Tables S6, S7, S8, and S9.

99

Table S6. Atom types and the Lennard-Jones parameters for nonbonded interactions. The color in table represents the color of atoms in the polymer molecules.

100

Pseudoatom	Group	Short form	Type Number	Mass	LJ potential well depth, ϵ/k_B [K]	LJ diameter, σ [\AA]	Partial charge, q [e]
CH ₃	Alkane	ch3	1	15.03450	98.0	3.75	0.00
CH ₂	Alkane	ch2	2	14.02658	46.0	3.95	0.00
CH	Alkane	ch	3	13.01864	10.0	4.68	0.00
C(C=)	Alkane	c	4	12.01070	0.5	6.40	0.00
C(=O)	Carbonyl	ccbn	5	12.01070	40.0	3.82	+0.40
O(=C)	Carbonyl	ocbn	6	15.99940	79.0	3.05	-0.40
O(-CH ₂)	Ether	oet	7	15.99940	55.0	2.80	-0.25
CH ₂ (-O-)	Ether	ch2et	8	14.02658	46.0	3.95	+0.25
C(CH-OH)	Alkane	c	9	12.01070	0.5	6.40	0.00
CH(-OH)	Alkane	chacl	10	13.01864	10.0	4.33	+0.515
O(-H)	Alcohol	oacl	11	15.99940	93.0	3.02	-0.70
H(-O)	Alcohol	hacl	12	1.007940	0.0	0.0	+0.435
O(-CH ₂)	Ether	oet	13	15.99940	55.0	2.80	-0.50
CH ₂ (-O-)	Ether	ch2et	14	14.02658	46.0	3.95	+0.25
CH ₃ (-O-)	Ether	ch3et	15	15.03450	98.0	3.75	+0.25
CH(=C-)	Alkene	chsp2	16	13.01864	47.0	3.73	0.00
C(=CH-)	Alkene	csp2	17	12.01070	20.0	3.85	0.00

101

102

Table S7. Bond parameters for 1-2 bonded interaction.

103

Bond	Type Number	Equilibrium bond length, r_0 [\AA]	Bond energy constant, k_l/k_B [K/\AA ²]
CH _x -CH _y	1	1.54	452500
CH _x -C(=O)	2	1.52	452500
C=O	3	1.20	704500
O-C(=O)	4	1.344	452500
O-CH ₂	5	1.41	452500
CH _x -CH(-OH)	6	1.54	452500
CH-O(-H)	7	1.43	452500
O-H	8	0.945	704500
O-CH(-OH)	9	1.41	452500
O-CH ₂	10	1.41	452500
O-CH ₃	11	1.41	452500
CH _x =CH _y	12	1.33	452500

Table S8. Angle parameters for 1-3 bonded interaction.

104

Angle	Type Number	Equilibrium angle, θ_0 [°]	Angle energy constant, k_θ/k_B [K/rad²]
CH _x -CH ₂ -CH _y	1	114.00	62500
CH _x -CH-CH _y	2	112.00	62500
CH _x -C-CH _y	3	109.47	62500
CH _x -C-C(=O)	4	109.47	62500
CH _x -C(=O)=O	5	126.00	40300
CH _x -C(=O)-O	6	111.00	35300
O(=C)=C-O	7	123.00	40300
C(=O)-O-CH ₂	8	115.00	62500
O-CH ₂ -CH _x	9	112.00	50300
CH _x -C-CH(-OH)	11	109.47	62500
CH _x -CH(-OH)-OH	12	109.47	50400
CH _x -CH(-OH)-O	13	112.00	50300
HO-CH-O	14	116.24	45350
CH(-OH)-O-CH ₂	15	112.00	60400
O-CH ₂ -CH _x	16	112.00	50300
CH(-OH)-O-CH ₃	17	112.00	60400
CH-O-H	18	108.50	55400
CH _x =(CH=)-CH _y	19	119.7	70420
CH _x =(C=)-CH _y	20	119.7	70420
CH _x -(C=)-CH _y	21	119.7	70420

105

106

Table S9. Dihedral parameters for 1-4 bonded interaction.

Torsion	Type Number	Angle energy constant,			
		c_0/k_B [K]	c_1/k_B [K]	c_2/k_B [K]	c_3/k_B [K]
CH _x -(CH ₂)-(CH ₂)-CH _y	1	0	355.03	-68.19	791.32
CH _x -(CH ₂)-(CH)-CH _y	2	-251.06	428.73	-111.85	441.27
CH _x -(CH)-(CH)-CH _y	3	-251.06	428.73	-111.85	441.27
CH _x -(CH ₂)-(C)-CH _y	4	0	0	0	461.29
CH _x -(CH ₂)-(C)-C(=O)	5	0	0	0	461.29
CH _x -(C)-C(=O)=O	6	2035.58	-736.9	57.84	-293.23
CH _x -(C)-C(=O)-O	7	-24.66	736.84	57.87	293.25
(C)-C(=O)-O-CH ₂ (-O-)	8	0.00	2158.00	2098.00	197.30
C(=O)-O-CH ₂ (-O-)-CH _x	9	0	725.35	-163.75	558.2
O=C(=O)-O-CH ₂ (-O-)	10	4715.99	-2194.00	2059.00	-153.40
O-CH ₂ (-O-)-CH _x -CH _y	11	0	176.62	-53.34	769.93
CH _x -(CH ₂)-(C)-CH(-OH)	12	0	0	0	461.29
CH _x -(C)-CH(-OH)-OH	13	1260.00	-630.00	781.20	0.00
CH _x -(C)-CH(-OH)-O	14	-251.06	428.73	-111.85	441.27
(C)-CH(-OH)-O-H	15	215.89	197.33	31.46	-173.92
(C)-CH(-OH)-O-CH ₂ (-O-)	16	0	725.35	-163.75	558.20
H-O-CH(-OH)-O	17	0	630.00	781.20	0.00
HO-CH(-OH)-O-CH ₂ (-O-)	18	4715.99	-2194.00	2059.00	-153.40
CH(-OH)-O-CH ₂ (-O-)-CH _x	19	0	725.35	-163.75	558.2
HO-CH(-OH)-O-CH ₃ (-O-)	20	4715.99	-2194.00	2059.00	-153.40
O-CH ₂ (-O-)-CH ₂ -CH _y	21	0	176.62	-53.34	769.93
(C)-CH(-OH)-O-CH ₃ (-O-)	22	0	725.35	-163.75	558.20
CH _x -C-CH=C	23	688.5	86.36	-109.77	-282.24
CH _x -CH ₂ =C-CH _y	24	Quadratic Potential, $U_{torsion}(\phi) = d_\phi(\phi - \phi_0)^2$ $d_\phi = 12400$ [K] (cis) = 13400 [K] (trans) $\phi_0 = \pi$ [rad] (cis) = 0 [rad] (trans)			

Section S6. Optimization of Simulation Parameters for Forcefield

115

116

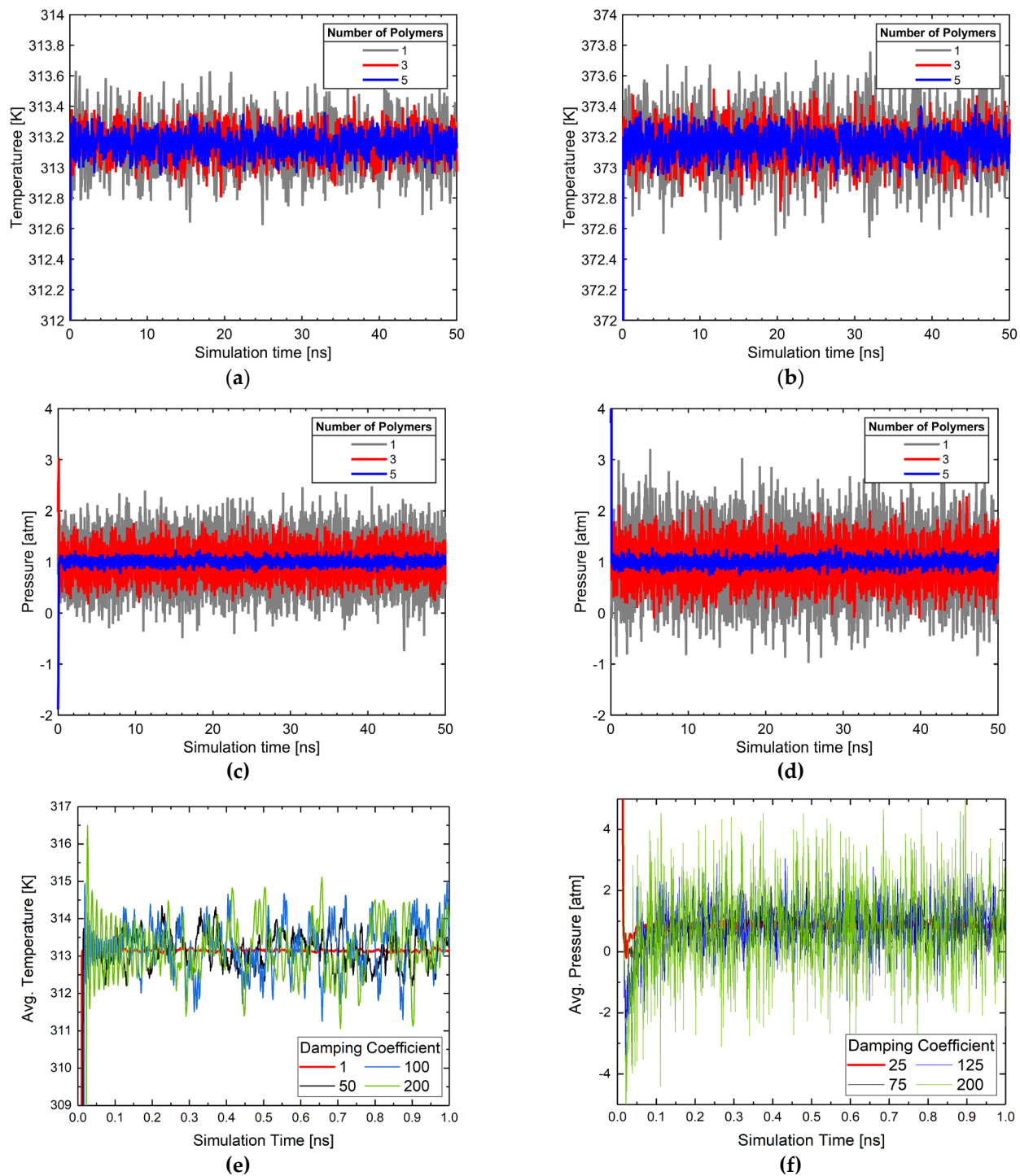


Figure S5. Optimization of simulation parameters for forcefield at 373.15 K and 1 atm: (1) temperature fluctuation over system size at (a) 40 °C and (b) 100 °C, (2) pressure fluctuation over system size at (c) 40 °C and (d), (e) average temperature for damping coefficients 1, 20, 100, and 200, and (f) average pressure for damping coefficients 1, 20, 100, and 200. This analysis suggested to use around 12000 UA atoms in the simulation box for each fluid to minimize the temperature and pressure fluctuation with damping coefficient of 1 for thermostat and 25 for barostat.

117

118

119

120

121

122

Section S7. Dependence of Viscosity on Simulation Parameters

Before simulating viscosity using time decomposition method [14], dependency of viscosity on important simulation parameters, such as correlation length, simulation time, and number of trajectories, were studied to report accurate and reliable viscosity from the simulations [14,15]. Figure S6 shows the average viscosity and standard deviation as a function of these important parameters. These parameters are arranged here in order of importance from top to bottom.

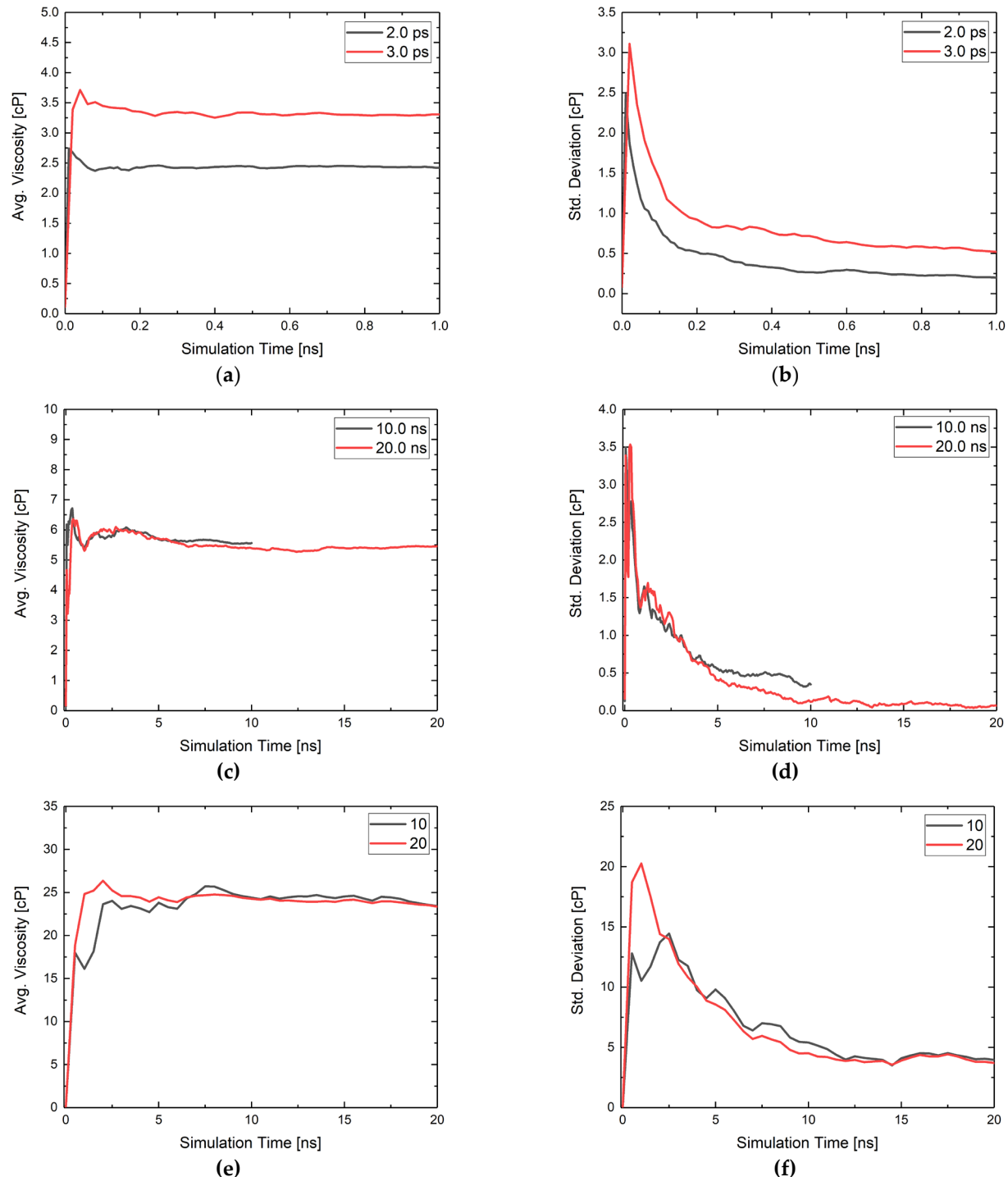
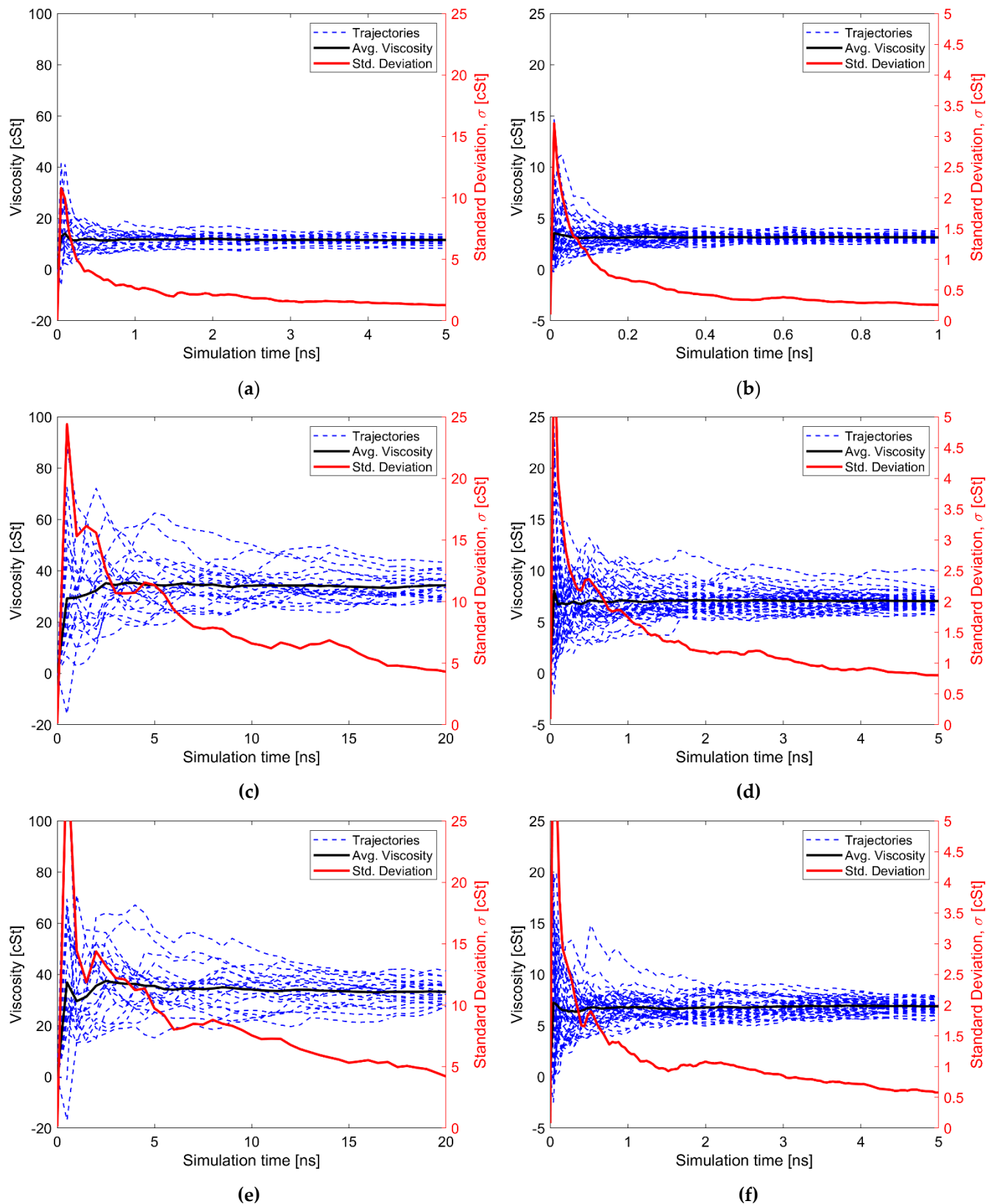


Figure S6. Dependence of viscosity on simulation parameters. These results suggest that (1) both average viscosity and standard deviation are highly dependent on the correlation length or time, (2) average viscosity is minutely but std. dev. is highly dependent on the simulation time, and (3) average viscosity and standard deviation are minutely dependent on the number of trajectories, but multiple trajectories are necessary for reporting reliable viscosity.

Section S8. Average Simulated Viscosity and Standard Deviation

134

135



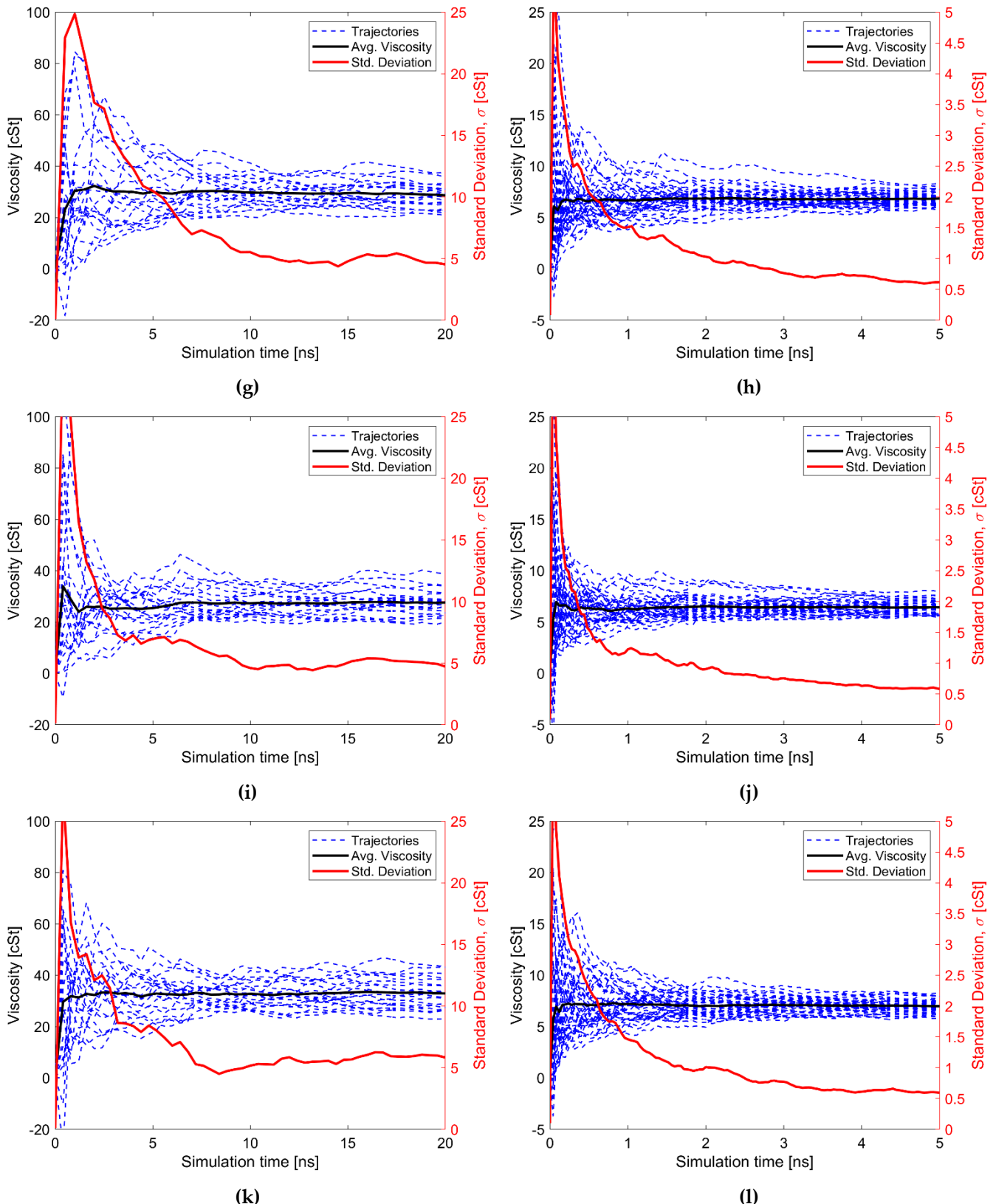


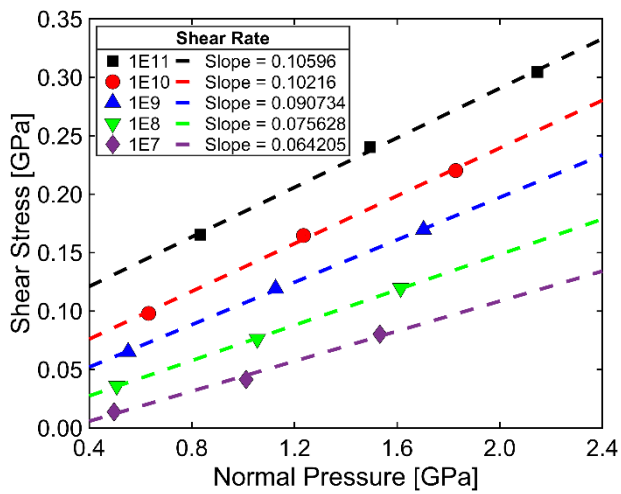
Figure S7. NVE trajectories with average viscosity and standard deviation curves of the following: (a) PAO 3 cSt at 40 °C, (b) PAO 3 cSt at 100 °C, (c) FKV-PAO at 40 °C, (d) FKV-PAO at 100 °C, (e) FKV-PIB at 40 °C, (f) FKV-PIB at 100 °C, (g) FKV-BDIP at 40 °C, (h) FKV-BDIP at 100 °C, (i) FKV-PAMA at 40 °C, (j) FKV-PAMA at 100 °C, (k) FKV-MABD at 40 °C, and (l) FKV-MABD at 100 °C. Blue dashed lines are NVE trajectories, black and red curves, respectively, represent the average viscosity and standard deviation calculated over these NVE trajectories as a function of simulation time.

136
137
138
139
140

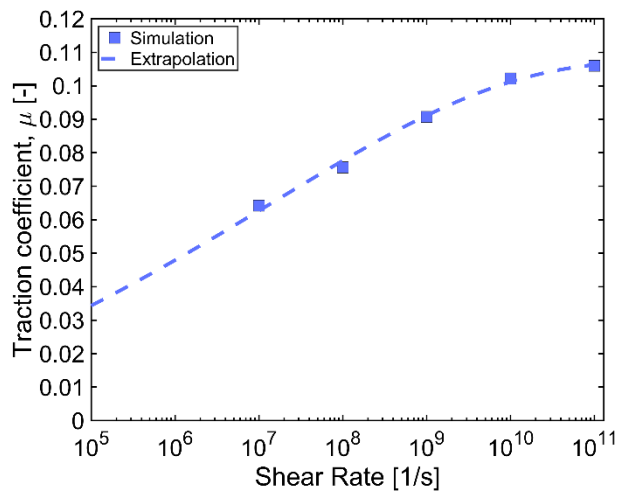
Section S9. Traction Coefficient and Extrapolated Traction Curves from Simulations

142

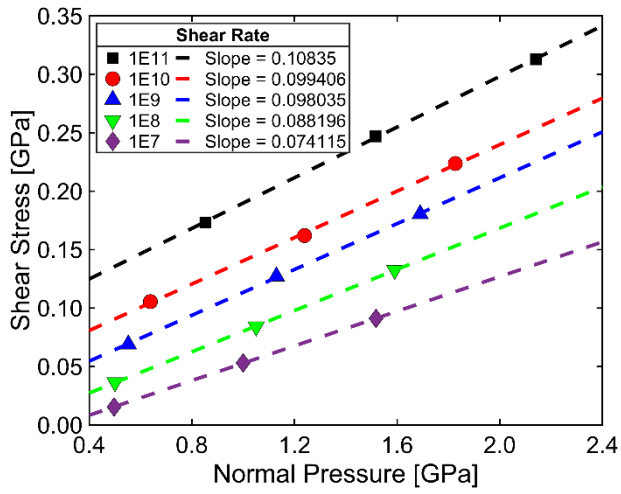
143



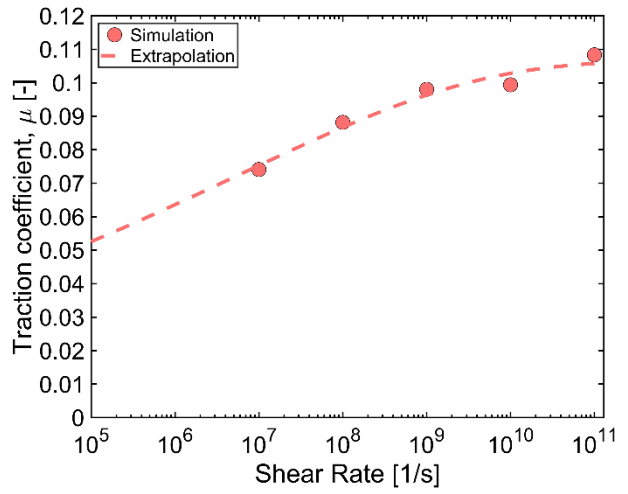
(a)



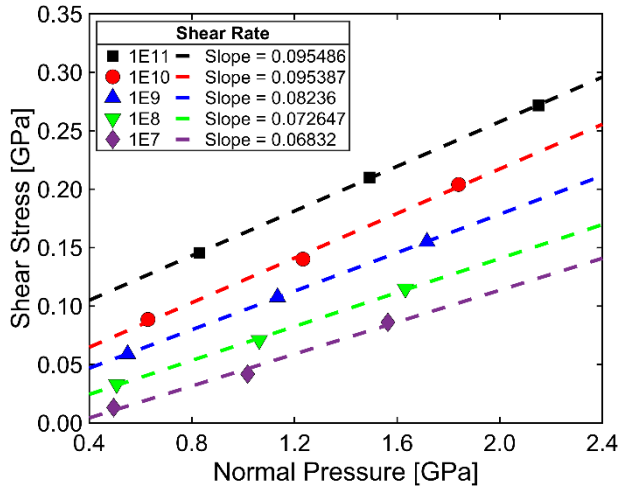
(f)



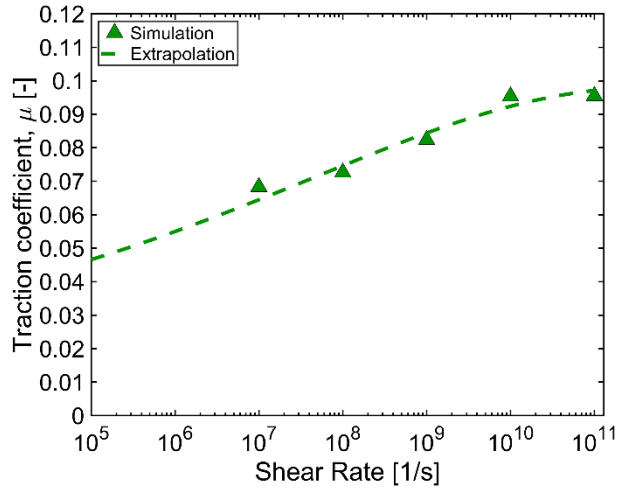
(b)



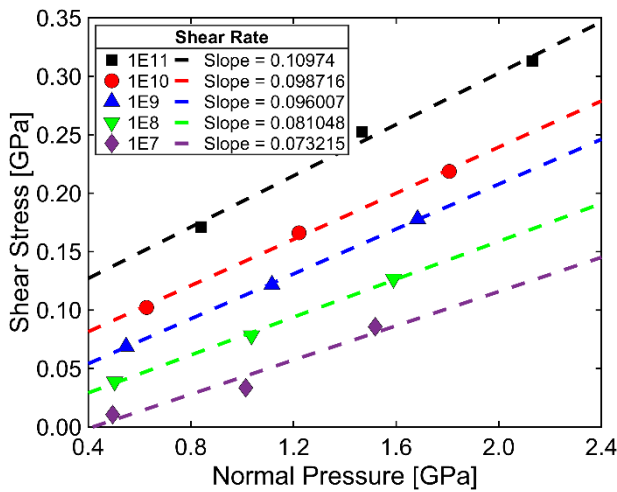
(g)



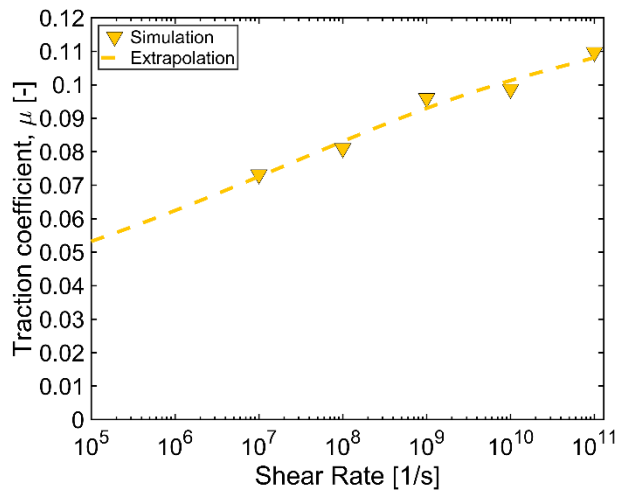
(c)



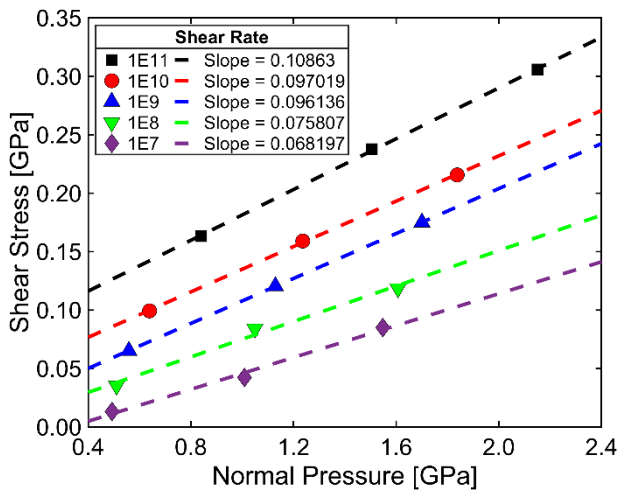
(h)



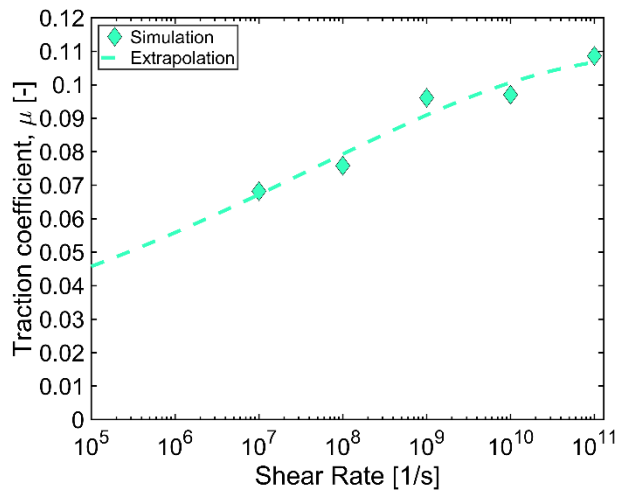
(d)



(i)



(e)



(j)

Figure S8. Traction coefficients at 40 °C directly calculated from the linear fit of the shear stress to the normal load or pressure of the following fluids: (a) FKV-PAO, (b) FKV-PIB, (c) FKV-BDIP, (d) FKV-PAMA, and (e) FKV-MABD. The black, red, blue, and green solid symbols, respectively, represent the shear stress as function of normal pressure at shear rates 1×10^{11} , 1×10^{10} , 1×10^9 , and 1×10^8 1/s. The black, red, blue, and green dash lines, respectively, represent the linear fit of shear stress to the normal pressure at shear rates 1×10^{11} , 1×10^{10} , 1×10^9 , and 1×10^8 1/s. The slopes of each linear fit are listed with their respective shear rates in the legend box. The extrapolated traction curve at 40 °C of the following fluids: (f) FKV-PAO, (g) FKV-PIB, (h) FKV-BDIP, (i) FKV-PAMA, and (j) FKV-MABD. The solid symbols represent the slopes as the traction coefficients calculated from the linear fit of simulation data of shear stress and normal load. The dashed line curves in these figures represent the extrapolated traction curve obtained by fitting the shear stress and normal pressure to the power function of shear rate.

144
145
146
147
148
149
150
151
152
153

154
155

Section S10. Governing Equations

10.1. End-to-end distance

In the physical chemistry study of polymers, the end-to-end vector is the vector that points from one end of a polymer to the other end. If each unit in a polymer is represented by a point in space, translation vectors \vec{r}_i connect between these joints. The end-to-end vector \vec{R} is the sum of these translation vectors [16,17]:

$$\vec{R} = \sum_i \vec{r}_i \quad (\text{S9})$$

The norm of the end-to-end vector is called the end-to-end distance R .

$$R = \sqrt{(x_{1st} - x_{last})^2 + (y_{1st} - y_{last})^2 + (z_{1st} - z_{last})^2} \quad (\text{S10})$$

10.2. Radius of Gyration

In polymer physics, the radius of gyration R_g is used to describe the dimensions of a polymer chain. The radius of gyration of a molecule at a given time is defined as [16,17],

$$R_g = \sqrt{\frac{1}{M} \sum_{i=1}^n m_i (r_i - r_{cm})^2} = \sqrt{\frac{1}{M} \sum_{i=1}^n m_i [(x_i - x_{cm})^2 + (y_i - y_{cm})^2 + (z_i - z_{cm})^2]} \quad (\text{S11})$$

Here, $M = \sum_{i=1}^n m_i$ and r_{cm} , respectively, are the total mass and center-of-mass position of the molecule and m_i and r_i , respectively, are mass and position of i^{th} atom. The center of mass r_{cm} of the molecule is calculated with the following formula [16,17].

$$r_{cm} = \frac{1}{M} \sum_{i=1}^n m_i r_i \quad (\text{S12})$$

or

$$x_{cm} = \frac{1}{M} \sum_{i=1}^n m_i x_i \quad y_{cm} = \frac{1}{M} \sum_{i=1}^n m_i y_i \quad z_{cm} = \frac{1}{M} \sum_{i=1}^n m_i z_i \quad (\text{S13})$$

10.3. Radius of Gyration Tensor

The gyration tensor of the conformations is defined as [16,17],

$$S = \frac{1}{M} \begin{bmatrix} \sum_{i=1}^n m_i (x_i - x_{cm})^2 & \sum_{i=1}^n m_i (x_i - x_{cm})(y_i - y_{cm}) & \sum_{i=1}^n m_i (x_i - x_{cm})(z_i - z_{cm}) \\ \sum_{i=1}^n m_i (x_i - x_{cm})(y_i - y_{cm}) & \sum_{i=1}^n m_i (y_i - y_{cm})^2 & \sum_{i=1}^n m_i (y_i - y_{cm})(z_i - z_{cm}) \\ \sum_{i=1}^n m_i (x_i - x_{cm})(z_i - z_{cm}) & \sum_{i=1}^n m_i (y_i - y_{cm})(z_i - z_{cm}) & \sum_{i=1}^n m_i (z_i - z_{cm})^2 \end{bmatrix} \quad (\text{S14})$$

10.4. Eigenvalues of Gyration Tensor and Shape Parameters

Since the gyration tensor S is a symmetric 3x3 matrix, a Cartesian coordinate system can be found in which it is diagonal (eigen) [16,17],

$$S = \begin{bmatrix} \lambda_x & 0 & 0 \\ 0 & \lambda_y & 0 \\ 0 & 0 & \lambda_z \end{bmatrix} \quad (\text{S15})$$

Here, the axes are chosen such that the diagonal elements are ordered $\lambda_x \leq \lambda_y \leq \lambda_z$. These diagonal elements are called the principal moments of the gyration tensor [16,17]. The squared radius of gyration is the sum of the principal moments, i.e., $R_g^2 = \lambda_x + \lambda_y + \lambda_z$ [16,17].

The three parameters that describe the shape can determined by the principal moments of the gyration tensor as [16,17],

1. Acylindricity (c),

$$c = \lambda_z - 0.5(\lambda_y + \lambda_x) \quad (\text{S16})$$

The acylindricity is always non-negative and zero only when the two principal moments are equal. The condition, $c = 0$ is met when the distribution of particles is cylindrically symmetric which can also be true when the particle distribution is symmetric with respect to the two coordinate axes, e.g., when the particles are distributed uniformly on a regular prism.

2. Asphericity (b),

$$b = \lambda_y - \lambda_x \quad (\text{S17})$$

It measures the deviation from the spherical symmetry. The asphericity is always non-negative and zero only when the three principal moments are equal. The condition, $b = 0$ is met when the distribution of particles is spherically symmetric which can also be true when the particles are distributed uniformly on a cube, tetrahedron or other Platonic solid.

3. relative shape anisotropy (k),

$$k = \frac{3}{2} \frac{\lambda_x^2 + \lambda_y^2 + \lambda_z^2}{(\lambda_x + \lambda_y + \lambda_z)^2} - \frac{1}{2} \quad (\text{S18})$$

It reflects both the symmetry and dimensionality of a polymer conformation. This parameter is limited between the values of 0 (if all points are spherically symmetric) and 1 (if all points lie on a line). It reaches 1 for an ideal linear chain and drops to zero for highly symmetric conformations. For planar symmetric objects, the relative shape anisotropy converges to the value of 1/4 [17].

10.5. Shear Rate at Mini Traction Machine (MTM) Test Condition

The regime of lubrication for a point contact was characterized by the dimensionless viscosity g_V and elasticity parameters g_E [18],

209
210
211
212

$$g_V = \frac{\alpha W^3}{(\eta_0 U)^2 R'^4} = 19.96E9 \quad (S19)$$

$$g_E = \frac{W^{8/3}}{(\eta_0 U)^2 E'^{2/3} R'^{10/3}} = 2.27E8 \quad (S20)$$

It was assumed that the pressure–viscosity (α) coefficient of the fluids is 15.7 1/GPa [19]. Then, the reduced radius of curvature (R'), reduced young's modulus (E'), contact area dimensions (a), average contact pressures (\bar{p}), maximum contact pressure (P_{max}), and maximum shear rate (τ_{max}) were determined using Equations (S21) - (S26) [18], respectively.

213
214
215
216

$$R' = R_b/2 \quad (S21)$$

$$E' = 2 \left(\frac{1 - v_b^2}{E_b} + \frac{1 - v_d^2}{E_d} \right)^{-1} \quad (S22)$$

$$a = (3WR'/E')^{1/3} \quad (S23)$$

$$\bar{p} = \frac{W}{\pi a^2} = 0.86 \text{ GPa} \quad (S24)$$

$$P_{max} \text{ or } P_H = \frac{3}{2} \bar{p} = 1.29 \text{ GPa} \quad (S25)$$

$$\tau_{max} = P_{max}/3 = 0.43 \text{ GPa} \quad (S26)$$

The central film thickness (h_c) for the point contact and compressible liquid can be derived using Hamrock-Dowson formulae as expressed by Equation (S27).

217
218

$$h_c = 1.55 \alpha^{0.53} (U \eta_0)^{0.67} E'^{0.061} R'^{0.33} P_H^{-0.201} = 0.121 \text{ } \mu\text{m} \quad (S27)$$

Finally, the shear rate was calculated by Equation (S28).

219
220
221

$$\dot{\gamma} = U \Sigma / h_c = 1.66 \times 10^6 \text{ s}^{-1} \quad (S28)$$

Section S11. Structure Properties of Polymers/Fluids from Molecular Dynamics Simulations

Listed in Table S10 are the 5 types of molecular weight and 17 structure parameters of the polymers which were studied in this project and, respectively, obtained from the chemistry of the polymers and MD simulations. These parameters were used in modeling VI and TE of the fluids.

Table S10. All 22 parameters of the polymers at 40 and 100 °C. These were used for VI and TE.

Temperature	40 °C						100 °C					
Parameter	PAO	PIB	BDIP	PAMA	MABD	ROMP	PAO	PIB	BDIP	PAMA	MABD	ROMP
M_w [kg/mol]	5.10	3.78	8.20	14.00	11.90	10.00	5.10	3.78	8.20	14.00	11.90	10.00
M_n [kg/mol]	5.00	2.10	3.00	8.50	4.30	15.00	5.00	2.10	3.00	8.50	4.30	15.00
M_{wt} [kg/mol]	5.05	2.13	16.26	32.56	11.17	9.88	5.05	2.13	16.26	32.56	11.17	9.88
M_{wb} [kg/mol]	1.01	1.00	13.05	3.34	2.48	5.00	1.01	1.00	13.05	3.34	2.48	5.00
M_{wp} [%]	20.03	47.11	80.24	10.26	22.20	49.57	20.03	47.11	80.24	10.26	22.20	49.57
L_x [Å]	36.29	26.33	109.08	85.43	62.25	107.18	36.05	24.04	94.32	99.20	51.28	97.89
L_y [Å]	40.86	27.35	49.36	52.53	57.33	45.45	35.51	26.31	82.33	56.69	82.70	47.87
L_z [Å]	37.19	23.55	152.31	58.54	67.26	65.65	37.16	24.76	125.89	58.13	75.95	63.36
R [Å]	43.40	29.32	38.70	44.57	68.01	41.14	31.17	26.38	55.92	60.96	87.02	47.63
R_g [Å]	14.78	12.31	51.96	23.96	25.55	35.03	14.13	11.74	43.96	28.18	32.09	33.46
$R_{g,xx}^2$ [Å ²]	69.38	56.62	730.20	369.55	213.96	895.32	66.34	42.71	576.33	580.46	119.31	795.94
$R_{g,yy}^2$ [Å ²]	83.11	60.04	106.22	100.17	171.97	79.49	60.49	53.39	320.63	113.76	523.50	95.02
$R_{g,zz}^2$ [Å ²]	68.35	39.98	1863.34	104.55	268.94	272.60	73.90	46.29	1042.15	100.79	444.16	240.81
$R_{g,xy}^2$ [Å ²]	33.75	10.41	-70.70	6.88	54.52	-139.99	14.09	2.42	256.35	-95.18	-42.70	126.52
$R_{g,xz}^2$ [Å ²]	13.55	0.98	-851.48	-39.16	-79.30	360.08	-5.14	0.48	-416.27	-35.34	-139.07	220.71
$R_{g,yz}^2$ [Å ²]	6.67	11.41	-22.64	-3.20	99.19	-47.06	-26.26	-3.59	-375.48	20.37	302.56	65.22
λ_x [Å ²]	160.26	120.76	2320.35	380.53	552.59	1125.32	135.37	105.86	1466.15	608.37	990.78	994.26
λ_y [Å ²]	38.88	26.44	301.88	100.69	61.60	76.16	44.31	26.71	337.71	106.03	64.16	87.02
λ_z [Å ²]	21.70	9.48	78.41	90.72	40.67	45.92	21.06	9.88	128.82	80.03	32.14	50.49
c [Å ²]	129.97	102.86	2130.21	283.66	501.45	1064.27	102.68	87.56	1232.88	515.04	942.63	925.50
b [Å ²]	17.19	16.97	223.48	11.18	20.93	30.24	23.24	16.83	208.89	25.34	32.01	36.53
k [-]	0.34	0.41	0.63	0.24	0.59	0.70	0.28	0.37	0.42	0.42	0.69	0.65

227

228

Listed in Table S11 are 17 structure parameters of the polymers at shear rates of 1.6×10^6 , 1×10^7 , 1×10^8 , 1×10^9 , 1×10^{10} , and 1×10^{11} 1/s. These parameters are the average of three normal pressure 0.5, 1.0, and 1.5 GPa at which TC simulations were executed. The 5 types of molecular weight are the same as listed in Table S10. These parameters were used in modeling TC of the fluids as a function of shear rate.

Table S11. All 17 parameters of the polymers at shear rates ranging from 1.6E6 to 1E11 1/s. These were used for TC.

Fluid	FKV-PAO						FKV-PIB					
Shear Rate [1/s]	1E11	1E10	1E9	1E8	1E7	1.6E6	1E11	1E10	1E9	1E8	1E7	1.6E6
L_x [Å]	62.56	53.82	50.49	53.30	48.19	38.03	56.27	49.70	45.83	48.98	45.31	32.61
L_y [Å]	28.33	31.01	34.32	34.94	40.28	32.88	17.18	18.43	19.78	20.36	21.13	23.19
L_z [Å]	19.09	20.21	20.94	22.23	24.47	32.35	14.21	14.75	14.87	15.97	16.48	22.43
R [Å]	45.94	37.54	37.40	44.80	43.65	27.60	46.83	40.43	35.54	42.57	39.28	34.86
R_g [Å]	17.66	15.65	15.28	16.52	16.09	12.86	17.40	15.57	14.77	15.97	15.01	12.81
$R_{g,xx}^2$ [Å ²]	270.44	187.36	157.89	188.24	151.65	73.76	298.60	228.01	193.71	232.38	188.49	92.97
$R_{g,yy}^2$ [Å ²]	40.53	49.24	65.04	70.08	89.31	47.68	20.37	22.71	28.97	30.27	33.34	36.20
$R_{g,zz}^2$ [Å ²]	17.20	18.61	19.24	21.46	26.91	45.80	12.11	13.01	13.08	16.21	17.00	41.90
$R_{g,xy}^2$ [Å ²]	0.61	-2.42	1.50	4.41	-9.68	6.95	-1.22	-2.31	1.05	-0.89	-13.17	4.26
$R_{g,xz}^2$ [Å ²]	30.56	20.41	15.70	14.45	4.42	19.78	27.45	18.16	15.21	20.21	17.46	3.52
$R_{g,yz}^2$ [Å ²]	0.15	-0.23	0.40	-5.15	1.93	0.35	-0.03	0.24	0.47	-0.78	0.96	2.94
λ_x [Å ²]	289.24	210.01	192.31	231.74	215.62	103.64	312.19	242.09	212.50	254.52	213.93	142.21
λ_y [Å ²]	29.56	34.28	38.10	35.39	37.04	40.90	14.53	16.54	17.75	18.79	18.73	20.82
λ_z [Å ²]	9.36	10.91	11.77	12.64	15.21	22.70	4.35	5.10	5.50	5.56	6.17	8.04
c [Å ²]	269.78	187.42	167.38	207.73	189.50	71.84	302.75	231.27	200.88	242.34	201.48	127.78
b [Å ²]	20.20	23.36	26.33	22.75	21.83	18.20	10.19	11.44	12.25	13.23	12.56	12.79
k [-]	0.62	0.50	0.45	0.53	0.46	0.19	0.74	0.68	0.64	0.65	0.65	0.51
Fluid	FKV-BDIP						FKV-PAMA					
Shear Rate [1/s]	1E11	1E10	1E9	1E8	1E7	1.6E6	1E11	1E10	1E9	1E8	1E7	1.6E6
L_x [Å]	725.72	711.25	927.13	584.46	493.52	141.63	199.95	131.53	127.79	113.41	106.49	86.08
L_y [Å]	45.32	48.12	52.16	52.12	61.68	108.75	42.85	49.10	50.53	51.70	48.66	47.97
L_z [Å]	21.17	21.98	21.52	27.44	39.49	152.42	28.20	35.68	37.64	39.69	47.95	46.40
R [Å]	544.42	552.57	829.83	132.77	179.32	200.85	136.46	76.87	66.84	59.62	55.94	49.06
R_g [Å]	220.10	225.08	295.34	160.33	124.98	57.98	53.48	33.11	32.66	29.73	27.60	24.27
$R_{g,xx}^2$ [Å ²]	54848.16	54877.86	88271.42	25619.62	15511.05	1297.90	3000.02	996.17	962.93	738.15	583.59	423.66
$R_{g,yy}^2$ [Å ²]	139.97	151.74	168.07	199.76	240.90	516.32	59.04	88.18	100.80	101.27	96.85	94.35
$R_{g,zz}^2$ [Å ²]	18.41	17.79	16.40	34.90	74.91	1548.13	30.09	53.03	58.88	61.90	96.20	70.90
$R_{g,xy}^2$ [Å ²]	-286.66	711.38	3288.45	727.84	374.06	629.94	14.61	-7.63	68.95	-63.43	-76.30	10.98
$R_{g,xz}^2$ [Å ²]	79.54	-31.51	556.94	752.46	877.64	1325.31	100.76	47.65	53.07	-33.47	105.33	-62.40
$R_{g,yz}^2$ [Å ²]	2.52	-9.67	22.95	41.81	44.14	722.73	0.60	-0.70	4.49	-0.01	-14.37	-10.74
λ_x [Å ²]	54929.80	54954.55	88402.26	25665.22	15577.98	3109.74	3017.42	1017.33	998.48	758.73	629.59	435.19
λ_y [Å ²]	64.38	80.65	42.73	179.76	233.63	166.74	50.54	84.77	84.70	98.07	95.54	96.00

λ_z [Å ²]	12.37	12.20	10.90	9.30	15.25	85.87	21.20	35.28	39.42	44.52	51.52	57.71
c [Å ²]	54891.43	54908.13	88375.45	25570.70	15453.54	2983.43	2981.55	957.31	936.42	687.44	556.06	358.33
b [Å ²]	52.01	68.45	31.83	170.47	218.38	80.87	29.35	49.49	45.28	53.55	44.02	38.29
k [-]	0.99	0.99	1.00	0.98	0.95	0.79	0.90	0.67	0.64	0.56	0.48	0.37
Fluid	FKV-MABD							F-ROMP				
Shear Rate [1/s]	1E11	1E10	1E9	1E8	1E7	1.6E6	1E11	1E10	1E9	1E8	1E7	1.9E6
L_x [Å]	145.10	108.06	113.18	91.77	99.36	61.98	313.60	284.76	169.92	218.31	64.56	106.78
L_y [Å]	33.61	40.08	38.67	47.07	45.13	70.46	30.70	34.45	52.17	48.13	64.22	38.47
L_z [Å]	22.97	26.51	26.19	28.85	28.93	41.87	21.71	21.64	26.47	25.64	59.34	44.96
R [Å]	101.04	68.37	68.36	66.60	77.30	59.64	255.14	234.93	110.51	165.40	53.43	38.32
R_g [Å]	41.47	29.83	31.81	25.70	28.07	23.41	92.46	84.49	50.26	62.62	24.16	33.07
$R_{g,xx}^2$ [Å ²]	1861.55	905.24	1030.18	570.53	710.20	274.15	9083.97	8518.87	2751.05	5879.82	236.49	964.80
$R_{g,yy}^2$ [Å ²]	45.30	71.95	63.74	100.76	93.62	209.71	37.25	62.64	141.08	113.96	178.28	54.41
$R_{g,zz}^2$ [Å ²]	22.69	31.46	29.29	38.21	29.77	75.92	21.59	18.92	30.50	29.29	204.41	111.56
$R_{g,xy}^2$ [Å ²]	1.23	-15.85	6.80	43.90	-46.05	128.60	46.89	-35.41	17.37	121.04	45.84	46.53
$R_{g,xz}^2$ [Å ²]	78.10	40.04	49.02	24.06	-0.25	-29.13	164.20	75.34	73.58	126.62	116.05	162.19
$R_{g,yz}^2$ [Å ²]	0.74	-0.88	-5.48	-15.93	-4.99	22.88	-0.12	1.80	-0.93	8.79	85.10	22.02
λ_x [Å ²]	1879.98	933.94	1056.14	615.76	742.25	453.49	9101.29	8533.53	2785.67	5916.00	478.61	1029.35
λ_y [Å ²]	36.83	57.26	50.15	72.12	69.15	68.48	31.36	54.17	121.44	86.11	95.95	60.48
λ_z [Å ²]	12.73	17.45	16.92	21.62	22.20	37.82	10.16	12.74	15.52	20.95	44.63	40.94
c [Å ²]	1855.20	896.58	1022.60	568.89	696.58	400.34	9080.54	8500.07	2717.19	5862.47	408.32	978.64
b [Å ²]	24.10	39.82	33.23	50.50	46.95	30.66	21.20	41.43	105.92	65.16	51.32	19.55
k [-]	0.86	0.69	0.74	0.56	0.63	0.51	0.98	0.88	0.78	0.74	0.37	0.71

Section S12. Test Fluid F-ROMP

To validate developed models of VI, TE, and TC, an addition fluid was formulated “F-ROMP.” Its composition and properties are listed in Table S12. This fluid was formulated by blending 5.8 wt.% of ROMP polymer with the blend of 48.1 wt.% of Nexbase 3.0 cSt and 39.6 wt.% of Nexbase 4.3 cSt lubricants as the base oil. Like the original five fluids, F-ROMP fluids were formulated with 6.5 wt.% of Anglamol 99 additive package. For the simulation purpose, since we did not know the structure of molecules of these Nexbase lubricants, we replaced Nexbase 3.0 cSt with previously formulated PAO 3.0 cSt (see Table S3) and Nexbase 4.3 cSt with a blend of 84.3 wt.% of PAO 4 cSt and 15.7 wt.% of PAO 8 cSt (viscosity of this blend of PAO 4 cSt and PAO 8 cSt is 4.28 cSt at 100°C = PAO 4.3 cSt). This composition of new base oils results in the same viscosity as the blend of Nexbase base oils. Therefore, the F-ROMP fluid model was developed in Material Studio software by mixing 5.8 wt.% of F-ROMP polymer, 51.7 wt.% of PAO3, and 42.5 wt.% of PAO4.3. Figure S9(a) and S9(b) shows the simulated and experimental kinematic viscosity both at 40°C and 100°C. These indicate that the new formulated fluid has viscosity close to what we have desired. All the properties of this new test fluid are listed in Table S13. Figure S9(c) shows the linear fit of shear stress to the normal pressure of simulation data at 40 °C and shear rates 1×10^{11} , 1×10^{10} , 1×10^9 , 1×10^8 , 1×10^7 , and 1×10^6 1/s. Figure S9(d) shows the extrapolated traction curve at 40 °C of the F-ROMP fluid.

Table S12. Composition of new test fluid F-ROMP.

Fluid ID		F-ROMP
Polymer $C_{704}H_{1410}$	ID	ROMP
	Mw [kg/mol]	15
	PDI	1.5
Polymer [wt.%]		5.8
Base Stock	Nexbase3030 [wt.%] \approx 3 cSt	48.1
	Nexbase3043 [wt.%] \approx 4 cSt	39.6
An glamol 99 additive package [wt.%]		6.5

Table S13. Measured and simulated properties of new test fluid F-ROMP.

Property	Experimental	Simulation
KV40 [cSt]	25.5	26.1 ± 4.1
KV100 [cSt]	5.6	5.8 ± 0.6
Viscosity Index	168.2	175.3
Thickening Efficiency @ 100°C [%]	9.96	10.35
Density @ 40°C [kg/m ³]	-	815.97
Density @ 100°C [kg/m ³]	-	778.41

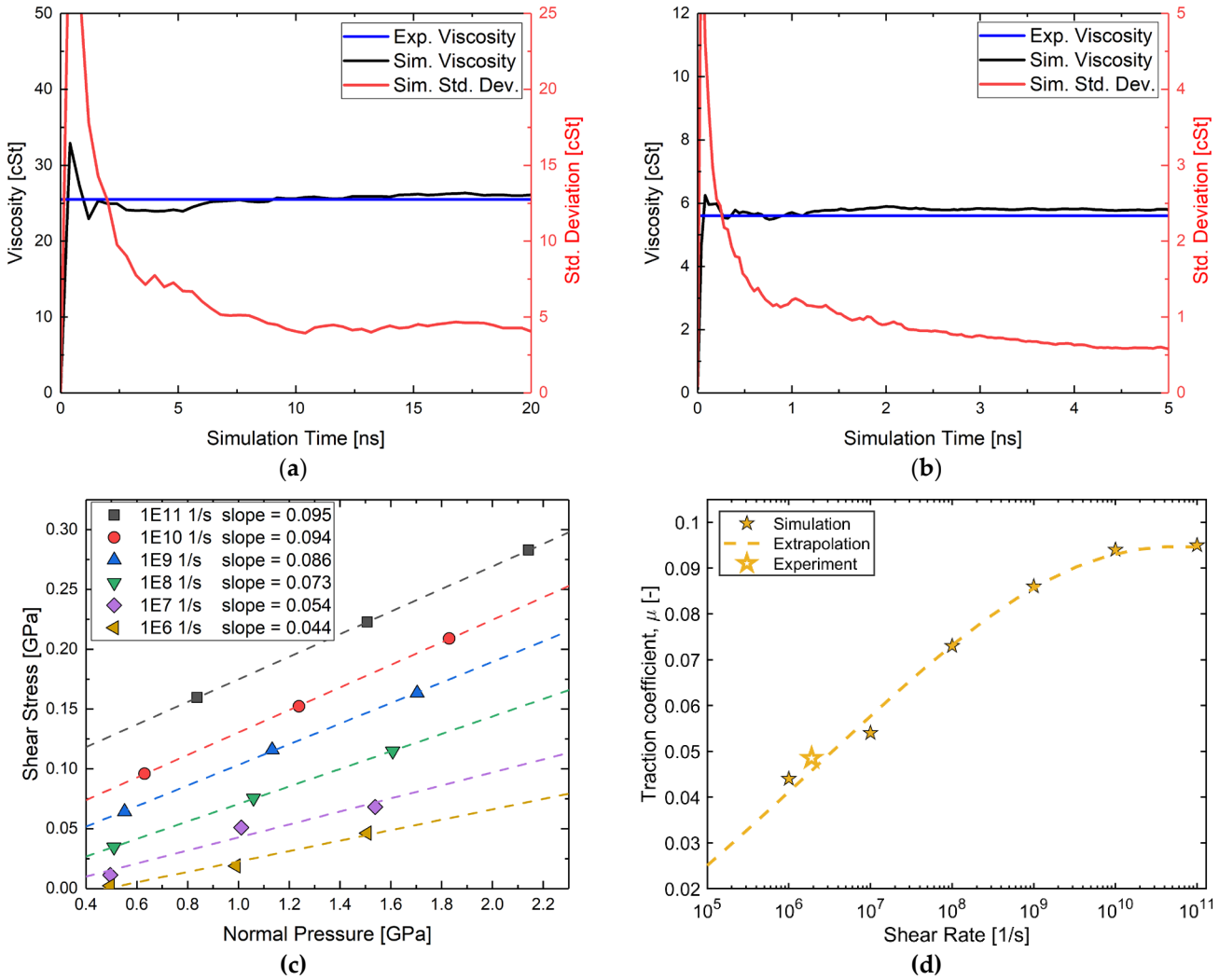


Figure S9. (a) Kinematic viscosity of fluid F-ROMP at 40 °C, (b) kinematic viscosity of fluid F-ROMP at 100°C, (c) the linear fit of shear stress to the normal pressure of simulation data of F-ROMP, the black, red, blue, green, purple, and orange dash lines, respectively, represent the linear fit of shear stress to the normal pressure at shear rates 1×10^{11} , 1×10^{10} , 1×10^9 , 1×10^8 , 1×10^7 , and 1×10^6 1/s. The slopes of each linear fit are listed with their respective shear rates in the legend box, and (d) the extrapolated traction curve of F-ROMP with the simulated and measured traction coefficients shown by the solid and hollow star symbols, respectively. The solid symbols represent the slopes as the traction coefficients calculated from the linear fit of simulation data of shear stress and normal load. The dashed line curves in the figure represents the extrapolated traction curve obtained by fitting the shear stress and normal pressure to the power function of shear rate.

256
257
258
259
260
261
262
263
264
265
266
267
268
269

References

- [1] PCS Instruments, 2014, "MTM2 Mini-Traction Machine" [Online]. Available: <https://pcs-instruments.com/wp-content/uploads/2014/03/MTM2.pdf>. 271
272
- [2] Grandelli, H. E., Dickmann, J. S., Devlin, M. T., Hassler, J. C., and Kiran, E., 2013, "Volumetric Properties and Internal 273
Pressure of Poly(α -Olefin) Base Oils," *Ind. Eng. Chem. Res.*, **52**(50), pp. 17725–17734. 274
- [3] Martin, M. G., and Siepmann, J. I., 1998, "Transferable Potentials for Phase Equilibria. 1. United-Atom Description of n- 275
Alkanes," *J. Phys. Chem. B*, **102**(14), pp. 2569–2577. 276
- [4] Martin, M. G., and Siepmann, J. I., 1999, "Novel Configurational-Bias Monte Carlo Method for Branched Molecules. 277
Transferable Potentials for Phase Equilibria. 2. United-Atom Description of Branched Alkanes," *J. Phys. Chem. B*, **103**(21), 278
pp. 4508–4517. 279
- [5] Wick, C. D., Martin, M. G., and Siepmann, J. I., 2000, "Transferable Potentials for Phase Equilibria. 4. United-Atom 280
Description of Linear and Branched Alkenes and Alkylbenzenes," *J. Phys. Chem. B*, **104**(33), pp. 8008–8016. 281
- [6] Chen, B., Potoff, J. J., and Siepmann, J. I., 2002, "Monte Carlo Calculations for Alcohols and Their Mixtures with Alkanes. 282
Transferable Potentials for Phase Equilibria. 5. United-Atom Description of Primary, Secondary, and Tertiary Alcohols," *J. 283
Phys. Chem. B*, **105**(15), pp. 3093–3104. 284
- [7] Kamath, G., Cao, F., and Potoff, J. J., 2004, "An Improved Force Field for the Prediction of the Vapor-Liquid Equilibria for 285
Carboxylic Acids," *J. Phys. Chem. B*, **108**(37), pp. 14130–14136. 286
- [8] Kamath, G., Robinson, J., and Potoff, J. J., 2006, "Application of TraPPE-UA Force Field for Determination of Vapor-Liquid 287
Equilibria of Carboxylate Esters," *Fluid Phase Equilibr.*, **240**(1), pp. 46–55. 288
- [9] Maerzke, K. A., Schultz, N. E., Ross, R. B., and Siepmann, J. I., 2009, "TraPPE-UA Force Field for Acrylates and Monte Carlo 289
Simulations for Their Mixtures with Alkanes and Alcohols," *J. Phys. Chem. B*, **113**(18), pp. 6415–6425. 290
- [10] Dinpajoooh, M., and Nitzan, A., 2020, "Heat Conduction in Polymer Chains with Controlled End-to-End Distance," *J. Chem. 291
Phys.*, **153**(16). 292
- [11] Ferrando, N., Gedik, I., Lachet, V., Pigeon, L., and Lugo, R., 2013, "Prediction of Phase Equilibrium and Hydration Free 293
Energy of Carboxylic Acids by Monte Carlo Simulations," *J. Phys. Chem. B*, **117**(23), pp. 7123–7132. 294
- [12] Clifford, S., Bolton, K., and Ramjugernath, D., 2006, "Monte Carlo Simulation of Carboxylic Acid Phase Equilibria," *J. Phys. 295
Chem. B*, **110**(43), pp. 21938–21943. 296
- [13] Yang, Y., Narayanan Nair, A. K., and Sun, S., 2020, "Sorption and Diffusion of Methane and Carbon Dioxide in Amorphous 297
Poly(Alkyl Acrylates): A Molecular Simulation Study," *J. Phys. Chem. B*, **124**(7), pp. 1301–1310. 298
- [14] Zhang, Y., Otani, A., and Maginn, E. J., 2015, "Reliable Viscosity Calculation from Equilibrium Molecular Dynamics 299
Simulations: A Time Decomposition Method," *J. Chem. Theory Comput.*, **11**(8), pp. 3537–3546. 300
- [15] Maginn, E. J., Messerly, R. A., Carlson, D. J., Roe, D. R., and Elliott, J. R., 2019, "Best Practices for Computing Transport 301
Properties 1. Self-Diffusivity and Viscosity from Equilibrium Molecular Dynamics [Article v1.0]," *Living J. Comput. Mol. 302
Sci.*, **1**(1), pp. 1–20. 303
- [16] Mattice, W. L., and Suter, U. W., 1994, *Conformational Theory of Large Molecules*, Wiley-Interscience, New York. 304
- [17] Theodorou, D. N., and Suter, U. W., 1985, "Shape of Unperturbed Linear Polymers: Polypropylene," *Macromolecules*, 305
18(6), pp. 1206–1214. 306
- [18] Bair, S., 2019, *High Pressure Rheology for Quantitative Elastohydrodynamics*, Elsevier. 307
- [19] Morgado, P. L., Echávarri Otero, J., Sánchez-Peña Lejarraga, J. B., Muñoz Sanz, J. L., Díaz Lantada, A., Muñoz-Guijosa, J. 308
M., Lorenzo Yustos, H., and Leal Wiña, P., 2009, "Models for Predicting Friction Coefficient and Parameters with Influence 309
in Elastohydrodynamic Lubrication," *Adv. Tribol.*, pp. 144–145. 310
- 311